Journal of Metals, Materials and Minerals, Vol. 31, No. 4, pp. 69-75, 2021

Formation of nano-crystalline chromium-zirconium nitride (Cr-Zr-N) film coating by DC unbalanced magnetron sputtering

Kumpon LEELARUEDEE[1], Kattareeya TAWEESUP[2], and Patama VISUTTIPITUKUL[1,*]

[1] *Metallurgical Engineering Department, Faculty of Engineering, Chulalongkorn University, Bangkok 10330, Thailand*
[2] *Department of Materials and Production Technology Engineering, Faculty of Engineering, King Mongkut's University of Technology North Bangkok, Bangkok 10800, Thailand*

***Corresponding author e-mail:** Patama.v@chula.ac.th

Received date:
18 June 2021
Revised date
6 September 2021
Accepted date:
6 September 2021

Keywords:
Nano-crystalline;
Cr-Zr-N;
Magnetron sputtering;
PVD;
Film-coating

Abstract

This research aimed to improve the properties of chromium nitride (CrN) film coatings by addition of zirconium (Zr) as the third element to form Cr-Zr-N ternary nitride. DC unbalanced magnetron sputtering method was used to form Cr-Zr-N film with various Zr/Zr + Cr atomic ratios. Mechanical properties, surface morphology and crystal structure of the film were investigated. In the research, Cr-Zr-N film were categorised into 3 types with different Zr amount: low zirconium, (Zr/Zr + Cr = 0.29), medium zirconium (Zr/Zr + Cr = 0.44), and high zirconium (Zr/Zr + Cr = 0.74). All Cr-Zr-N films exhibited nano-crystalline structures with lower surface roughnesses than those of crystalline CrN film. With Zr addition, the highest hardness of Cr-Zr-N coating layer increased to 1762.7HV, in the *low Zr* film. Likewise, Young's modulus value increased from 213.9 GPa for the Cr-N film to 269.0 GPa for the *low Zr* film. Both surface hardness and Young's modulus slightly decreased when the amount of Zr in the ternary Cr-Zr-N film increased. The nano-crystalline Cr-Zr-N film exhibited better adhesion comparing to the binary Cr-N film. Scratch test showed the increased critical load (LC_1) from 1.91 N for the CrN film to 3.21 N for the ternary Cr-Zr-N film.

1. Introduction

Steels have been widely used in diverse applications, including as structural parts in construction, dies and molds in production, and so on [1,2]. The properties of steels have been improved by several methods, including surface coating. One of the coating techniques, which has become of interest recently, is physical vapor deposition (PVD), which can provide several coating materials at a low temperature and can minimize environmental burdens [3,4]. PVD provides coating layer with various properties such as high surface hardness, excellent tribological properties and corrosion resistance [5-8]. Durability of film coated by PVD can be improved by controlling film structure and surface treatment prior to PVD [9,10]. Among various types of coating materials, chromium nitride (CrN) has been widely investigated as a protective coating due to its high level of hardness, excellent corrosion resistance and high oxidation resistance. However, the most important limitation of CrN usage is its degradation at temperatures above 700°C. The structure of the CrN film formed by PVD has been reported to be columnar, which weakens some properties, such as the corrosion resistance of the film [11-16]. Many attempts have been performed to improve the properties of the coating film, including adjusting the coating parameters to avoid the formation of a columnar structure or forming a ternary nitride (A-B-N). There have been some reports that ternary nitrides, such as Cr-Ti-N, Cr-Al-N and Cr-W-N, have better properties than the CrN binary nitride, especially their thermal stability at temperatures above 700°C [17-23]. In this research zirconium (Zr) was selected as a ternary alloy to make the Cr-Zr-N ternary nitride, since ZrN has a good thermal and chemical stability, high mechanical strength and good corrosion resistance [24-29]. Moreover, the addition of Zr into other alloy systems, such as Cu alloys, has been reported to promote the formation of a refined microstructure [30,31]. Although the formation of Cr-Zr-N has been reported, there have been no reports on formation and properties of nano-crystalline Cr-Zr-N [32].

In this research, the formation of a thin film of ternary nitride, in the form of Cr-Zr-N, was studied. The effect of the Zr amount added into the ternary nitride (as the Zr:Cr atomic ratio) on the structure, phase formation and mechanical properties were also investigated.

2. Experimental procedure

2.1 Sample preparation

H13 tool steel was heat treated at 1000°C for 90 min, quenched in oil and then tempered twice at 550°C for 60 min. Subsequently, it was cut into disk shape pieces (25 mm diameter and 3 mm thickness), polished until 1 μm alumina, rinsed in acetone and kept in desiccator.

2.2 Coating

Samples were rinsed in acetone and attached in the sample holder of an unbalanced magnetron sputtering chamber with Cr and Zr targets. Evacuation of the coating chamber was performed using a rotary

and turbomolecular pump until the pressure reached 5.5×10^{-5} torr. Then, argon (Ar) was introduced to the chamber with a flow rate of 40 sccm until the pressure reached the working pressure (8.5×10^{-3} torr). The coating process started with Ar ignition for achieving a stable plasma, then nitrogen (N_2) was filled into the chamber. Since the heat of atomization of Zr (603.59 kJ·mol^{-1}) is much higher than that of Cr (395.74 kJ·mol^{-1}), the sputtering rate of the Zr target was much lower than that of the Cr target [33]. As a result, target poisoning was more likely to occur at the Zr target. In order to avoid poisoning at the Zr target, the N_2 flow rate was reduced from 5 sccm when coating with CrN to 4 sccm for the Cr-Zr-N coatings. The current at the Cr and Zr targets was varied so as to control the Cr:Zr ratio in the resulting ternary nitride film. The coating parameters are listed in Table 1, while the electrical current and gas flow rates utilized are shown in Table 2. Since the constant current mode is selected for the power supplies, the voltages of the targets range from 300 V to 370 V. According to those parameters, samples can be categorized into 4 groups: no zirconium (NZ), low zirconium (LZ), medium zirconium (MZ) and high zirconium (HZ).

2.3 Characterization

The microstructure of the coated samples was observed by a JEOL, model JSM-7100F, Field-emission scanning electron microscopy (FE-SEM) and a JEOL, model JEM 2100, Transmission electron microscope (TEM), while the surface roughness and morphology were observed by atomic force microscopy (AFM), Veeco model Dimension 3100. Ratio of Zr and Cr was measured by Energy Dispersive Spectrometer (EDS, Oxford Inca PentaFETx3). Phase and crystal structure were investigated by glancing incident angle X-ray diffraction (GIXRD, Rigaku D/Max 2200P/C) using CuK$_\alpha$ radiation with an incident angle of 3 deg.

Hardness of the coating layer was measured by the Nano indentation test (Hysitron, Triboscan). In order to avoid any effect from the substrate, the penetration depth of the indenter was limited to less than 10% of the film thickness. The coating film adhesion was assessed by scratch tests using a starting load of 1 N. The scratch load kept increasing until it reached 30 N. The distance for the scratch test was fixed at 40 mm with a stylus traveling speed of 50 μm·s^{-1}.

3. Results

3.1 Phase and microstructure

The average hardness of the H13 sample after heat treatment, as measured by Vickers' microhardness using a load of 10 g, was 525.4 HV, which confirms the existence of tempered martensite in the sample after heat treatment. The coated sample changed from a shiny metallic to a grey color. All coating layer homogeneously covers entire surface as can be seen in Figure 1. Thin metallic interlayer, having approximately 100 nm thickness, formed by Ar plasma prior to nitride coating, can be observed in the cross-section microstructure. The total layer thickness of NZ (718 nm) is thinner than those of LZ, MZ and HZ layer (1424 nm, 1421 nm and 1673 nm, respectively), due to the single target operation with low applied current. Increasing of Zr contents provides higher sputtering rate, resulting in the highest growth rate of HZ layer. Growth rates of layers with Zr addition in this experiment range from 0.26 nm·s^{-1} of LZ to 0.31 nm·s^{-1} of HZ which were around two-folds faster than that of NZ layer (0.13 nm·s^{-1}).

Table 1. Coating parameters.

Parameters	Details
Base pressure	5.5×10^{-5} torr.
Working pressure	8.5×10^{-3} torr.
Pre-sputtering	Ar gas, 15 min
Coating time	90 min
Pure Ar	99.99% purity
Pure N_2	99.99% purity
Voltage	300 V to 370 V
Growth temperature	Room temperature

Table 2. Electrical current and gas flow rate.

Sample	Current at Cr target (A)	Current at Zr target (A)	Nitrogen flow rate (sccm)	Argon flow rate (sccm)
NZ	0.4	-	5	40
LZ	0.4	0.4	4	40
MZ	0.3	0.7	4	40
HZ	0.2	0.7	4	40

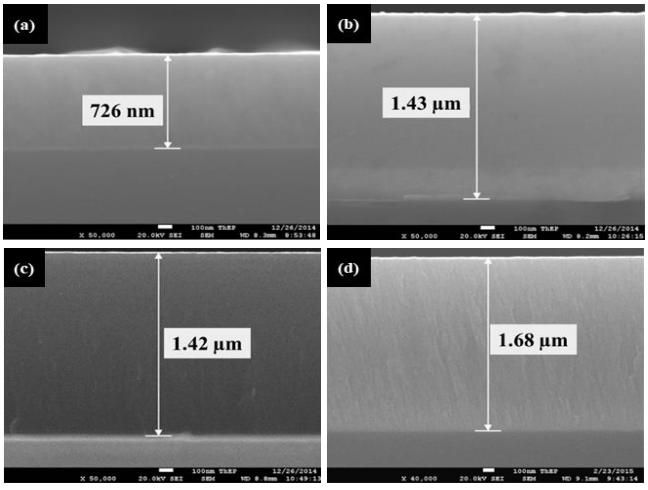

Figure 1. Cross-sectional microstructure of the coating layer, as revealed by SEM analysis, for the (a) NZ (b) LZ, (c) MZ, and (d) HZ.

EDS analysis (Figure 2) assures presence of Cr, Zr and N in LZ, MZ and HZ layer, while only Cr and N were detected in NZ layer. Amount of Zr in the layer increased with increasing Zr current as can be seen that Zr/(Zr + Cr) ratio increases from 0.29 to 0.44 and 0.74 for LZ, MZ and HZ, respectively. Noted that the applied current at the Zr target was much higher than that at the Cr target due to the higher heat of atomization of Zr (603.59 kJ·mol^{-1}) than Cr (395.74 kJ·mol^{-1}) [33]. The higher heat of atomization of Zr leads to a lower Zr sputtering rate, although this can also be caused by poisoning of the Zr target due to reaction of N_2 and the Zr target surface. The Gibb's free energy of formation for ZrN (-481.2 kJ·mol^{-1}) is 2.1-fold lower than that for CrN (-229.5 kJ·mol^{-1}) [34] and so the Zr target has a higher risk of poisoning. To avoid this, the N_2 flow rate was reduced from 5 sccm (for CrN coating) to 4 sccm for the ternary Cr-ZrN coatings.

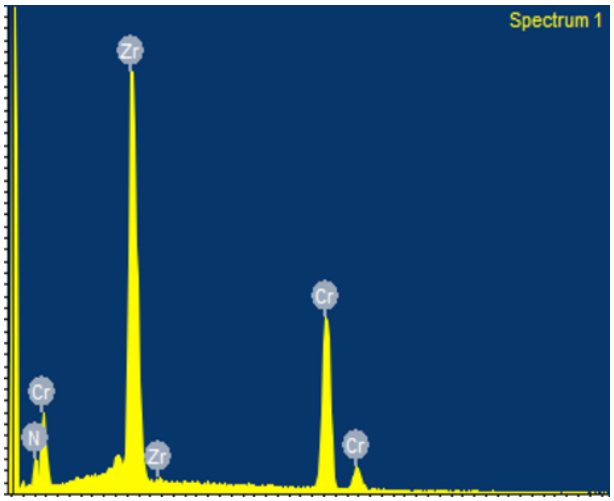

Figure 2. Representative EDS profile of the 0.8:1 Cr: Zr ratio (sample No. 3).

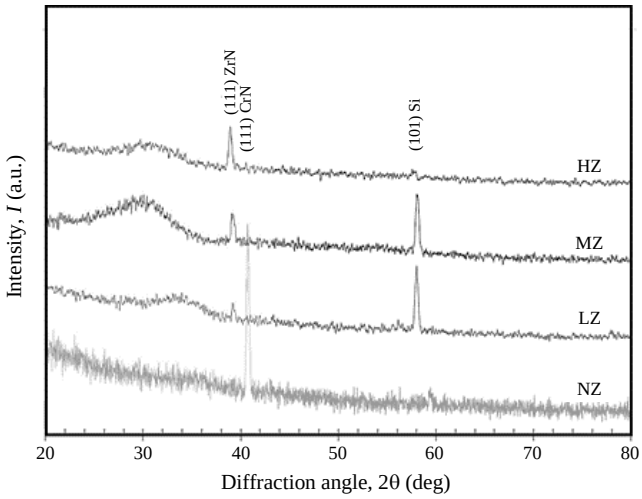

Figure 3. GIXRD profiles of (a) NZ (b) LZ, (c) MZ, and (d) HZ.

The GIXRD profiles of the layers are shown in Figure 3. The results revealed formation of crystalline CrN on NZ layer whereas broadened peak at a diffraction angle (2θ) of around 30 degree to 36 degree was detected in LZ, MZ and HZ layer. The disappearance of CrN peak in the LZ, MZ and HZ layer will be discussed later. The broadened peaks reflect that atoms in the film do not have enough periodicity to be detected by the GIXRD. The average crystallite size of the coating layer calculated by Scherrer equation is equal to 4.07 nm. Microstructure observed by TEM of MZ samples (Figure 4) confirms formation of nanocrystalline structure with average crystal size of 9.1 nm and 2.8 nm for standard deviation (STD). The histogram of crystal size distribution in the MZ sample is presented in Figure 5. The interplanar distance was approximately 0.26 nm which accorded to the d-spacing of (111) plane of CrN and ZrN mixture.

According to GIXRD result, increasing of Zr amount in Cr-Zr-N film shifts the broadened peaks to a lower angle which indicates an increasing of lattice parameter. This can be explained by substitution of large Zr atoms (diameter of 159 pm) for Cr atoms (124 pm) resulting in an enlarged lattice parameter and increased randomness of the crystal structure [35]. The Zr atoms added into the Cr-Zr-N film also blocks growth of grain. Therefore, amount of Zr in the Cr-Zr-N film plays an important role in the formation of nano-crystalline structure. Indeed, addition of the third element such as Zr, B, and Nb has been reported in other systems that these additional atoms can retard atomic diffusion which increases the plausibility of fine featureless and nano-crystalline formation. Another factor that supports the formation of a nano-crystalline structure is a high cooling rate. Since the thin film coating by PVD in this research did not use any auxiliary heater or any bias voltage at the substrate, the substrate temperature was comparatively low (less than 90°C by measuring a dummy sample), leading to a low atomic mobility on the surface [22,30,36]. Combining these two plausible reasons, the nano-crystalline Cr-Zr-N can be fabricated by optimization of the Zr amount and lowering the substrate temperature. Schematic illustration of film formation mechanism is shown in Figure 6.

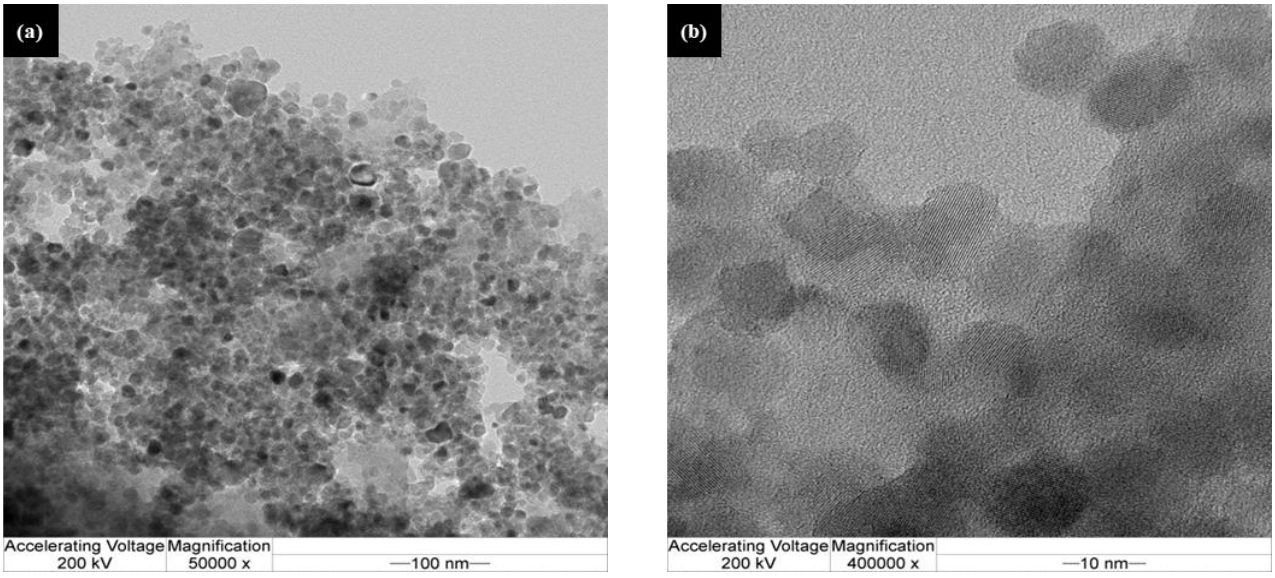

Figure 4. TEM microstructure (Left) and HR-TEM (Right) of MZ sample.

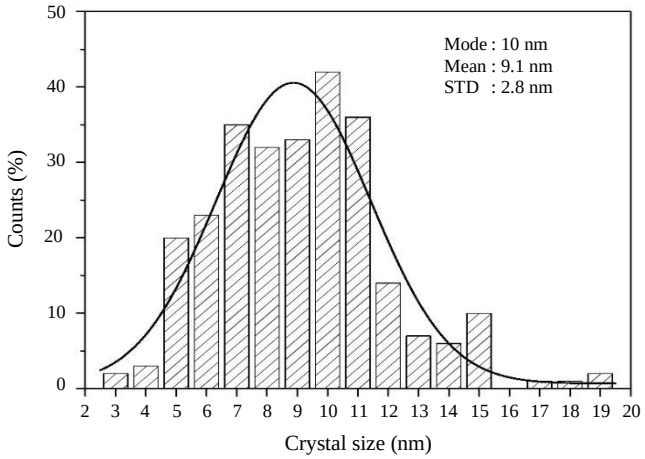

Figure 5. Crystal size distribution in the MZ sample.

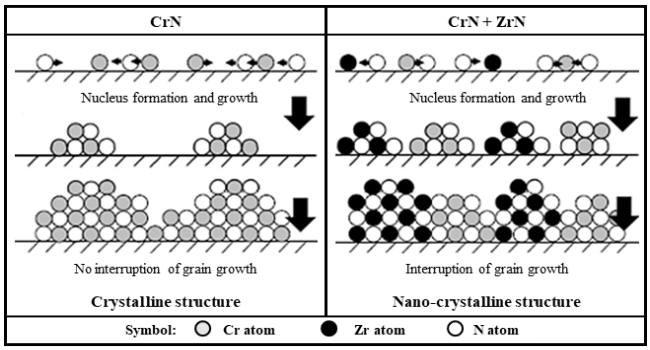

Figure 6. Schematic illustration of film formation mechanisms.

The surface morphology of the coating layer, as observed by AFM, showed a reduced surface roughness with increasing amounts of Zr in the coating layer (Figure 7), decreasing from a roughness average (R_a) of about 2.4 nm in the NZ film to 1.6 nm in the LZ film and to 1.4 nm for HZ film. Likewise, the root mean square roughness (R_{rms}) was also reduced in the same trend, from 3.2 nm in the NZ film down to 2.0 ± 0.08, 1.9 ± 0.05 and 1.8 ± 0.06 nm in the Cr-Zr-N films with LZ, MZ and HZ film, respectively. Thus, the formation of fine crystals in the LZ, MZ and HZ layer reduced the surface roughness, in comparison with the coarse crystals in NZ layer. This result agreed with Z. Xin *et al.* report, which revealed that surface roughness of film tended to reduce with the fine structure [37].

3.2 Mechanical properties

The proportion of Zr in the Cr-Zr-N film is not only affected the surface morphology but also mechanical properties of the coating layer due to the formation of a nano-crystalline structure as shown in Table 3.

Hardness and Young's modulus, as measured by the Nano indentation test with a limited penetration depth to eliminate any effect from the substrate. The load and displacement curves of MZ were shown in Figure 8. To confirm the reliability of test results, the measurements were done at least 3 times. The maximum depth is limited to 10 percent of the coating thickness in order to avoid the substrate effect. For MZ coatings, the penetration depth was set to be 130 nm. The loading path shows elastic and plastic behavior while the unloading path shows the elastic behavior of the coatings. Hardness of the coating were calculated by these behaviors. The slopes of unloading paths were employed in Young's modulus calculation [38]. In this research, Young's modulus values of the coatings were calculated by using Triboscan software, according to Equation 1 and 2.

$$\frac{1}{E^*} = \frac{1-\upsilon^2}{E} + \frac{1-\upsilon'^2}{E'} \quad (1)$$

Where, E^* is the reduced elastic modulus, E is Young's modulus of the coating, E' is Young's modulus of the indenter, υ is poisson ratio of coating, and, υ' is poisson ratio of the indenter.

$$E^* = \frac{dP}{dh}\frac{1}{2h_p}\frac{1}{\beta}\sqrt{\frac{\pi}{24.5}} \quad (2)$$

Where, E^* is the reduced elastic modulus, $\frac{dP}{dh}$ is slope of unloading path, h_p is the peak depth, and, b is the indenter constant.

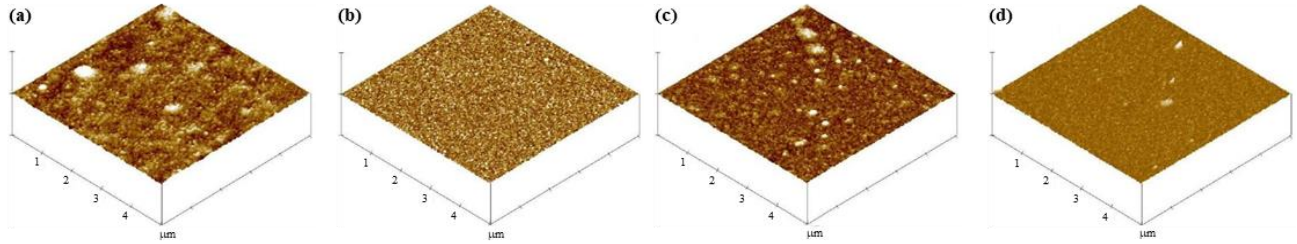

Figure 7. Surface morphology (AFM analysis) (a) NZ and (b-d) the Cr-Zr-N films with (b) LZ, (c) MZ, and (d) HZ.

Table 3. Properties of the coating film.

Sample	Zr/(Zr+Cr) ratio	Surface roughness (nm)		Critical load (N)		Hardness (HV)	Young's modulus (GPa)
		R_a	R_{rms}	LC_1	LC_2		
NZ	0	2.4	3.2	1.91	6.69	1290.1	213.9
LZ	0.29	1.6	2.0	2.95	6.37	1762.7	269.0
MZ	0.44	1.4	1.9	3.21	6.12	1610.8	253.6
HZ	0.74	1.4	1.8	2.18	6.55	1451.3	229.2
H13	-	-	-	-	-	525.4	-

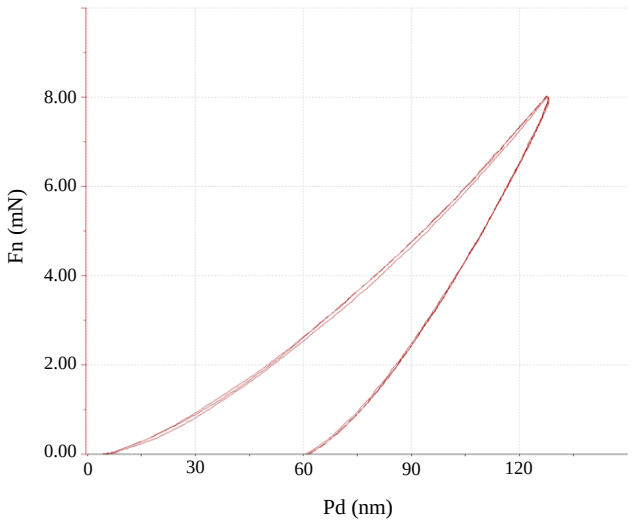

Figure 8. Load and displacement curves of MZ sample.

The measured hardness of the coating layer increased from 1290.1 HV of NZ sample to 1762.7 HV of LZ sample. However, increasing amount of Zr slightly decreases hardness. Likewise, the Young's modulus also increased from 213.9 GPa of NZ sample to 269.0 GPa of LZ sample, then decreased at higher Zr levels. The decreasing of hardness of nanocrystalline CrZrN film with increasing Zr content is due to the lower hardness of ZrN than that of CrN [39]. The adhesion of the coating film was higher in the Cr-Zr-N films than the CrN one, as seen by the increasing LC_1 from 1.91 N for NZ sample to the maximum value of 3.21 N for MZ sample. This can be explained by the definition of LC_1, which is the critical load when the first crack forms in the coating layer. Figure 9 shows relation of Young's modulus and critical load (LC_1 and LC_2). Films with high hardness and Young's modulus values can endure crack formation resulting in a higher LC_1 value. However, after the crack forms they have a low ductility, and so only a small amount of plastic deformation can occur and this results in the delamination (low LC_2 value) of the nanocrystalline Cr-Zr-N film from the H13 substrate.

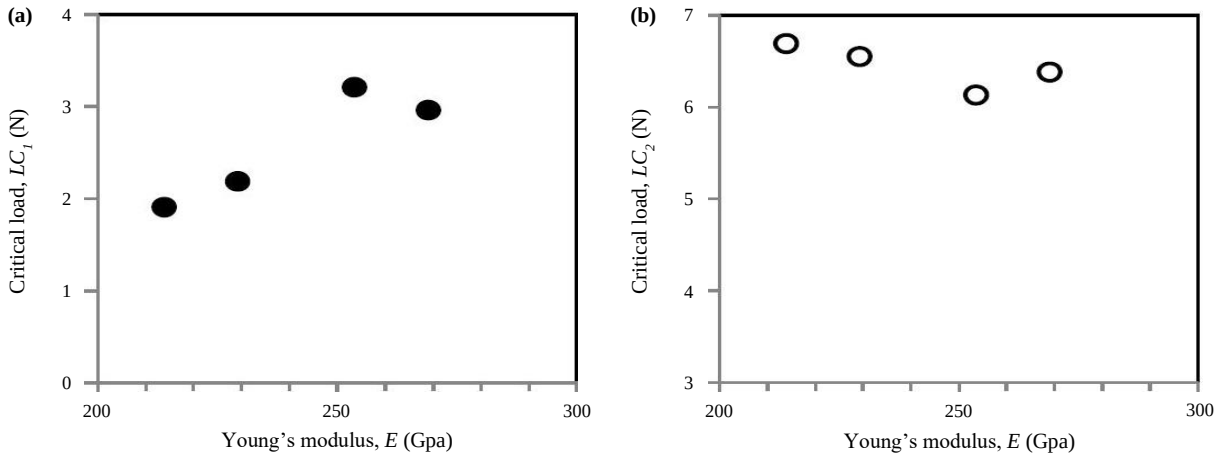

Figure 9. Relation of the critical load, (a) LC_1, and (b) LC_2, with the Young's modulus.

4. Conclusions

Nanocrystalline ternary nitride films, comprised of Cr-Zr-N at different Zr: Cr ratios, were fabricated by unbalanced DC Magnetron sputtering. The nanocrystalline film formation was seemingly due to limited atomic diffusion caused by the Zr atoms acting as a barrier and also by the low substrate temperature. The amount of Zr added into the CrN could be increased up to a 2.8:1 atomic ratio of Zr:Cr. The surface hardness and Young's modulus of nanocrystalline Cr-Zr-N films were higher than in the binary Cr-N film by about 36.6% and 28.5%, respectively. The surface roughness of the Cr-Zr-N coating layer was also reduced compared to that for CrN, while the adhesion of the coating layer, in terms of the LC_1, was increased due to the higher hardness and Young's modulus of the nanocrystalline film. However, the LC_2 did not remarkably change upon the addition of Zr to CrN.

Acknowledgements

The authors would like to express their gratitude to Thai Parkerizing company for their helps on scratch test.

References

[1] W. F. Smith, *Structure and properties of engineering alloys*. Mc. Graw Hill; U.S.A., 1993.

[2] E. J. Miola, S.D. de Souza, M. Olzon-Dionysio, D. Spinelli, and C. A. dos Santos, "Nitriding of H-12 tool steel by direct –current and pulsed plasmas," *Surface and Coating Technology*, vol. 116-119, pp. 347-351, 1999.

[3] D. M. Mattox, *Handbook of physical vapor deposition (PVD) processing*. U.S.A.: Noyes publication, 1998.

[4] K. Wasa, M. Kitabatake, and H. Adachi, *Thin Film Materials Technology*, New Jersey: William Andrew publishing, 2004.

[5] A. Thakur, S. Gangopadhyay, K. P. Maity, and S. K. Sahoo, "Evaluation on effectiveness of CVD and PVD coated tools during dry machining of incoloy825," *Tribology Transactions*, vol. 61, pp. 1048-1058, 2016.

[6] A. Vadiraj, M. Kamaraj, and R.Gnanamorrthy, "Fretting wear studies on PVD TiN coated, ion implanted and thermally oxidized biomedical titanium alloys," *Surface Engineering*, vol. 23, pp. 209-215, 2007.

[7] L. E. Gil, S. Liscano, P. Goudeau, E. Le Bourhis, E. S.Puchi-Cabrera, and M. H. Staia, "Effect of TiAlN PVD coatings on corrosion performance of WC-6% Co," *Surface Engineering*, vol. 26, pp. 562-566, 2010.

[8] M. Beger, and M Larsson, "Mechanical properties of multilayer pvd Ti/TiB_2 coatings," *Surface Engineering,* vol. 16, pp. 122-126, 2000.

[9] E. Zoestbergen, and J. Th. M. De Hosson, "Crack resistance of PVD coatings: Influence of surface treatment prior to deposition," *Surface Engineering*, vol. 18, pp. 283-288, 2002.

[10] G. S. Fox-Rabinovich, K. Yamamoto, B. D. Beake, I. S. Gershman, A. I. Kovalev, S.C. Veldhuis, M. H. Aguirre, G. Dosbaeva, and J. L. Endrino, "Hierarchical adaptive nano-structured PVD coatings for extreme tribological applications: the quest for nonequilibrium states and emergent behaviour," *Science and Technology of Advanced Materials,* vol. 3, pp. 1-26, 2012.

[11] A. Ehiasarian, W. D. Munz, L. Hultman, U. Helmersson, and I. Petrov, "High power pulsed magnetron sputtered CrNx films," *Surface and Coating Technology*, vol. 163, pp. 267-272, 2003.

[12] J. Mo, M. Zhu, A. Leyland, and A. Matthews, "Impact wear and abrasion resistance of CrN, AlCrN and AlTiN PVD coating," *Surface and Coating Technology,* vol. 215, pp. 170-177, 2013.

[13] N. Abukhshim, P. Mativenga, and M. Sheikh, "Heat generation and temperature prediction," *International Journal of Machine Tools and Manufacture,* vol. 46, pp. 782-800, 2006.

[14] T. Polcar, T. Kubart, R. Novak, and P. Stroky, "Comparison of tribological behavior of TiN, TiCN and CrN at elevated temperatures," *Surface and Coating Technology,* vol. 193, pp. 192-199, 2005.

[15] G. Bertrand, C. Savall, and C. Meunier, "Properties of reactively RF magnetron-sputtered chromium nitride coating," *Surface and Coating Technology*, vol. 96, pp. 323-329, 1997.

[16] D. Mercs, N. Bonasso, S. Naamane, J. M. Bordes, and C. Coddet, "Mechanical and tribological properties of Cr–N and Cr–Si–N coatings reactively sputter deposited," *Surface and Coating Technology,* vol. 200, pp. 403-407, 2005.

[17] S. M. Aouadi, K. C. Wong, K. A. R. Mitchell, F. Namavar, E. Tobin, D. M. Mihut, and S. L.Rohde, "Characterization of titanium chromium nitride nanocomposite protective coatings," *Applied Surface Science,* vol. 229, pp. 387-394, 2004.

[18] H. Hasegawa, M. Kawate, and T. Suzuki, "Effects of Al contents on microstructures of Cr_{1-X} Al_XN and $Zr_{1-X}Al_XN$ films synthesized by cathodic arc method," *Surface and Coating Technology,* vol. 200, pp. 2409-2413, 2005.

[19] P. Hones, R. Sanjines, and F. Levy, "Sputter deposited chromium nitride based ternary compounds for hard coatings," *Thin Solid Films,* vol. 332, pp. 240-246, 1998.

[20] K. H. Lee, C. H. Park, Y. S. Yoon, and J. J. Lee, "Structure and properties of $(Ti_{1-X}Cr_X)N$ coatings produced by the ion-plating method," *Thin Solid Films,* vol. 385, pp. 167-173, 2001.

[21] J. J. Nainaparampil, J. S. Zabinski, and A. Korneyi-Both, "Formation and characterization of multiphase film properties of (Ti–Cr)N formed by cathodic arc deposition," *Thin Solid Films,* vol. 333, pp. 99-94, 1998.

[22] Z. T. Wu, Z. B. Qi, D. F. Zhang, B. B. Wei, and Z.C.Wang, "Evaluating the influence of adding Nb on microstructure, hardness and oxidation resistance of CrN coating," *Surface and Coating Technology,* vol. 289, pp. 45-51, 2016.

[23] D. Chaliampalias, N. Pliatsikas, E. Pavlidou, K. Kolaklieva, R. Kakanakov, N. Vouroutzis, P. Patsalas, E. K. Polychroniadis, K. Chrissafis, and G. Vourlias, "Compositionally gradient PVD CrAlSiN films: structural examination and oxidation resistance," *Surface Engineering,* pp. 1-7, 2016.

[24] Z. G. Zhang, O. Rapaud, N. Banosso, D. Mercs, C. Dong, and C. Coddet, "Microstructures and corrosion behaviors of Zr modified CrN coatings deposited by DC magnetron sputtering," *Vacuum,* vol. 82, pp. 1332-1336, 2008.

[25] S. M. Aouadi, T. Maeruf, R. D. Twesten, D. M. Mihut ,and S. L. Rohde, "Physical and mechanical properties of chromium zirconium nitride thin films *Surface and Coating Technology,* vol. 200, pp. 3411-1417, 2006.

[26] G. Kim, B. Kim, S. Lee, and J. Hahn, "Structure and mechanical properties of Cr–Zr–N films synthesized by closed field unbalanced magnetron sputtering with vertical magnetron sources," *Surface and Coating Technology,* vol. 200, pp. 1669-1675, 2005.

[27] C. Chantharangsi, S. Denchitcharoen, S. Chaiyakun, and P. Limsuwan, "Structure and surface morphology of Cr-Zr-N thin films deposited by reactive dc magnetron sputtering," *Procedia Engineering,* vol. 32, pp. 868-874, 2012.

[28] K. Kim, H. Kim, J. La, and S. Lee, "Effects of interlayer thickness and the substrate material on the adhesion properties of CrZrN coatings," *Japanese Journal of Applied Physics,* vol. 55, pp. 01AA02, 2016.

[29] R. W. Harrison, and W. E. Lee, "Processing and properties of ZrC, ZrN and ZrCN ceramics: a review," *Advances in Applied Ceramics,* vol. 115, pp. 294-307, 2016.

[30] X. Shi, J. Zhang, and M. Sun, "Role of Zr in icosahedral forming in Cu–Zr metallic glasses," Materials Letters, vol. 157, pp. 180-182, 2015.

[31] M. Naka, M. Miyake, M .Maeda, I. Okamoto, and Y. Arata, "High corrosion resistance of amorphous Co-Cr-Mo-Zr alloys," *Scripta Materialia,* vol. 17, pp. 1293-1297, 1983.

[32] C. Chantharangsi, S. Denchitcharoen, S. Chaiyakun, and P. Limsuwan, "Structures, morphologies, and chemical states of sputter-deposited CrZrN thin films with various Zr contents," *Thin Solid Films,* vol. 589, pp. 613-619, 2015.

[33] M. Harmelin, J. Bigot, and M. Lasocka, *Thermal stability of Cu-Zr-M glasses as a function of an average atomization enthalpy,* in: S. Steeb, H. Warlimont (Eds.) Rapidly Quenched Metals, Elsevier, 1985, pp. 335-338.

[34] M. Binnewies, and E. Milke, *Thermochemical Data of Elements and Compounds,* Weinheim :Wiley-VCH., 2002.

[35] S. Khamseh, and H. Araghi, "A study of the oxidation behavior of CrN and CrZrN ceramic thin films prepared in a magnetron sputtering system," *Ceramics International,* vol. 42, pp. 9988-9994, 2016.

[36] O. Jiminez, M. Audronis, A. Leyland, M. Flores, E. Rodriquez, K Kanakis, and A Matthew, "Small grain size zirconium-based

coatings deposited by magnetron sputtering at low temperatures," *Thin Solid films,* vol. 591, pp. 149-155, 2015.

[37] Z. Xin, S. Xiao-Hui, and Z. Dian-Lin, "Thickness dependence of grain size and surface roughness for dc magnetron sputtered Au films," *Chinese Physics B.,* vol. 19 pp. 086802, 2010.

[38] W. C. Oliver, and G. M. Pharr, "An improved technique for determining hardness and elastic modulus using load and displacement sensing indentation experiments," *Journal of Materials Research*, vol. 7, pp. 1564-1583, 2011.

[39] O. Maksakova, A. Pogrebnjak, and V. Beresnev, "Features of Investigations of Multilayer Nitride Coatings Based on Cr and Zr," *Uspehi Fiziki Metallov,* vol. 19, pp. 25-48, 2018.